Hindawi Publishing Corporation
Journal of Structures
Volume 2013, Article ID 138617, 8 pages
http://dx.doi.org/10.1155/2013/138617

Research Article

Finite Element Modeling of Mode I Failure of the Single Contoured Cantilever CFRP-Reinforced Concrete Beam

T. Nicholas,[1] D. Boyajian,[2] S. E. Chen,[1] and A. Zhou[1]

[1] *University of North Carolina at Charlotte, Charlotte, NC 28223, USA*
[2] *Indiana Wesleyan University, Upland, IN 46989, USA*

Correspondence should be addressed to T. Nicholas; tnichola@uncc.edu

Received 20 February 2013; Revised 13 October 2013; Accepted 12 November 2013

Academic Editor: Domenico Bruno

The single contour cantilever beam (SCCB) test method has been developed with the intent to capture Mode I opening failures of CFRP-reinforced concrete beams. Recent development in the method explores possible shifting damage into the concrete substrate by using the International Concrete Repair Institute (ICRI) Surface Profile Level Three (SP3) as the desired CFRP bonded interface to concrete. To validate and explain the interface fracture behavior, finite element analysis using special cohesive elements has been performed. The cohesive element allows separation of the concrete substrate from the CFRP. This paper presents the simulation of laboratory test results, where failure in the substrates has been successfully reproduced. The simulation results indicate that finite element method using cohesive elements can successfully replicate Mode I critical strain energy release rate and the peak capacity of the laboratory tests and may have the potential to simulate actual applications.

1. Introduction

Several laboratory methodologies have been developed over the past few years to measure Mode I critical strain energy release rate involving composite wrapped concrete beams. Failures of representative methodologies designed to isolate Mode I opening failure of a fracture interface include the modified double cantilever beam (DCB) method [1], the peel test method [2], the membrane peeling method [3], and the single contour cantilever beam (SCCB) method [4]. All the above methods are variations of each other with different strengths and weaknesses, depending on the application. However, the SCCB method exclusively ensures that the failure will always be the first mode. A second advantage of the SCCB method is the elimination of compliance measurements.

The SCCB method was first developed by Boyajian [5] and has been utilized to determine the critical strain energy release rates at the bonding interface between concrete and carbon fiber-reinforced polymer (CFRP) [4, 6, 7]. Figure 1 shows the schematics of the SCCB test including the test specimen that consists of concrete base plate, CFRP bonded layer, the wood contour, and the experimental setup that includes a steel strap for pulling on the wood contour. Figure 2(a) shows the actual test setup within a MTS test apparatus with arrow indicating the direction of pull load. With the SCCB test, the high tensile capacity LVL is loaded with a normal force, P, inducing Mode I failure behavior of the CFRP to concrete interface and thus avoiding the arm break-off failure. The starter crack is created by debonding the CFRP from the concrete substrate for the first fifty millimeters of the bond length. This is achieved by pretreating the starter crack location with a substrate with tape or wax paper. The starter crack can be seen in Figure 2(c) as the white shaded area on the substrate.

The current study focused on using the International Concrete Repair Institute Surface Preparation 3 (ICRI SP3) [8] method to ensure failure within the substrate. In order to achieve the necessary surface profile, the ICRI standards allow for shot blasting, sand blasting, or pressurized water to be used. After numerous trials, the surface preparation method that produced the most consistent results was pressurized water from a 34.47 MPa pressure washer. Additionally, a set of surface profile tabs were obtained to assist in classifying the surface. The surface profile tabs are raised surface, rubber square swatches which illustrate each of the

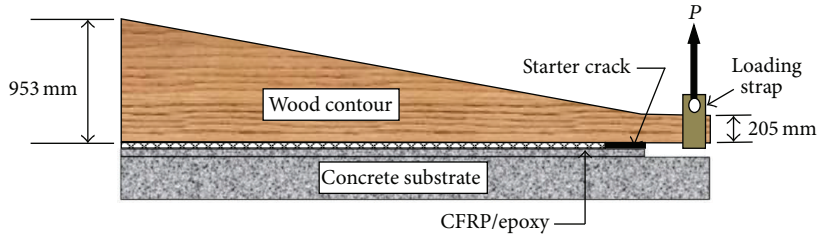

Figure 1: Schematic of single contoured cantilever beam test.

(a) SCCB test setup

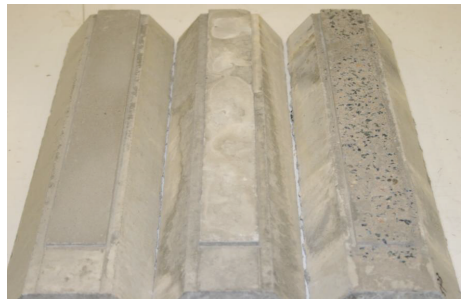

(b) Concrete surfaces (left to right): SP1, mould, and SP3

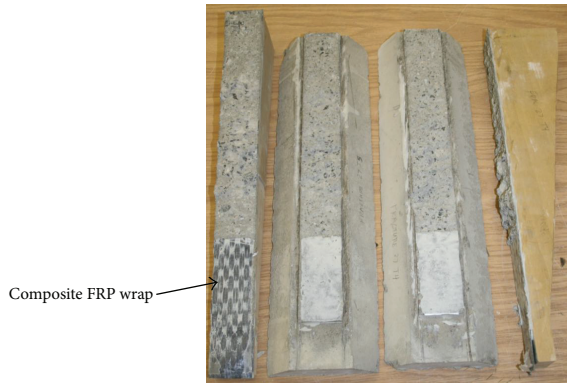

(c) Failed specimen showing exposed substrate

Figure 2: The SCCB test: (a) experimental setup (arrow indicating load direction); (b) different concrete surfaces (SP1, mould, and SP3); (c) interface surface of failed specimens: FRAC1031_T1 and FRAC1031_T2.

ICRI surface profiles. The common method for classifying the surface is to check the target surface tab (SP 3), as well as, the tab above (SP 4) and the tab below (SP 2). Figure 2(b) shows the different surface areas: SP1, mould, and SP3. Study of failure in the substrates is important as it may lead to premature failure and brittle failures [9]. Figure 2(c) shows the failed specimens clearly indicating failure within concrete substrate.

This paper reports finite element (FE) simulation of a series of SCCB tests conducted with concrete specimens prepared with SP3 surfaces, which was not previously attempted. In order to develop realistic FE models, a damage evolution approach has been adopted. The results presented shows that the approach effectively predicts the critical strain energy release rate of the bonded interface. The model also compares well with the laboratory test results.

2. Mode 1 Fracture

Fracture behavior can normally be characterized as beginning with crack initiation and intensifying through crack propagation. At the onset of crack initiation, the crack propagation behavior becomes a function of the displacement of the failed interface surfaces [10–12]. Irwin [13] defined three failure modes to describe how the surfaces are displaced by Mode I, Mode II, and Mode III failures. Mode I describes a failure of the interface bond that occurs normal to the failed surface, often referred to as the opening mode. While most fractures can be described by one of the failure modes, the mixing of mode failures, such as Mode I-Mode II, is also a possibility. The ability of an engineering material to resist these failure modes is frequently referred to as fracture toughness. The commonly accepted method for representing fracture toughness is the critical release strain energy, G_C, as defined by the Irwin-Kies equation [13, 14]:

$$G_C = \left(\frac{P_C^2}{2b}\right)\left(\frac{dC}{da}\right), \quad (1)$$

where G_C is the critical strain energy release rate (J/m^2), P_C is the critical load (N), b is the width of the specimen (mm), and dC/da is the rate of compliance (C) with respect to crack length (a) (N^{-1}).

3. Analytical Modeling of Fracture and the Cohesive Elements

As it pertains to the current study, finite element modeling of the SCCB can be divided into two categories: compliance of the SCCB wood contour and fracture. As there exist a number of methods to model crack propagation, it is important to select an efficient and accurate representation of the failure behavior. While the SCCB has not specifically been modeled for fracture, a number of past studies have focused on the fracture of the double cantilever beam and the peel test. Most recently, Nicholas [15], Huang and Lyons [16], and Diehl [17]

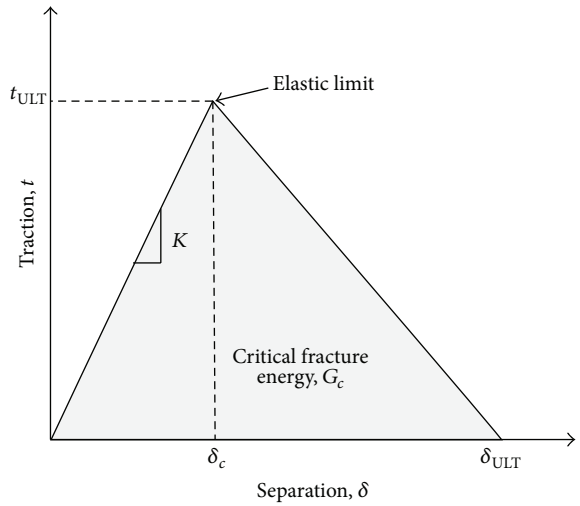

FIGURE 3: Damage evolution curve for ABAQUS cohesive element (t (MPa), δ (mm)) [18].

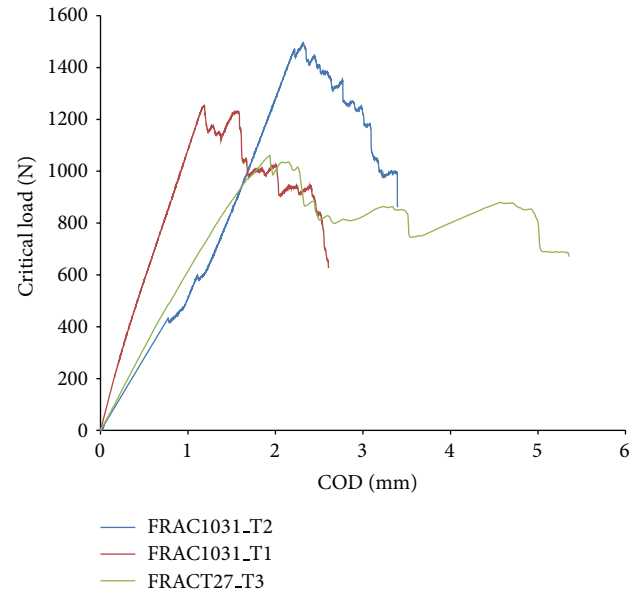

FIGURE 4: Critical strain energy curves for representative specimens.

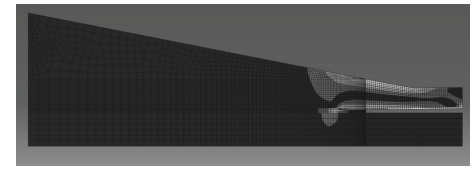

FIGURE 5: Finite element model of the SCCB utilizing cohesive element.

proposed methodologies for modeling the DCB, a modified DCB, and a peel test, respectively. For each study, the model was used to determine the total energy required to propagate the crack tip. The total energy required to fracture concrete can be taken as

$$G_f = \frac{1}{B * (W - a)} \int P d\delta, \tag{2}$$

where G_f is the specific fracture energy (J/m^2), B is the specimen thickness (mm), W is the fracture width (mm), a is the initial crack length (mm), P is the point load (N), and δ is the displacement perpendicular to crack length (mm).

Huang and Lyons [16] employed the J-integral algorithm in ABAQUS to model the crack propagation of a modified DCB as well as to calculate the critical strain energy release rate. The methodology produced good results compared to the basic energy equation and laboratory results. However, according to Nicholas [15], the cohesive element is an efficient approach to modeling fracture, as well, when the crack propagation is known *a priori*.

Diehl [17] proposed utilizing an ABAQUS cohesive element to model the bonded region between elastic and inelastic materials, namely, a thin film. In the study, a penalty-based approach to debonding was proposed. In the penalty approach or damage evolution, as the elements ultimate stress capacity (traction (MPa), t_{ULT}) is achieved, the element is deleted from the model and does not provide further resistance to load. This damage process is illustrated in Figure 3, where the ultimate nominal stress serves as the elastic limit and the area under the curve provides the critical fracture energy, G_c. This "unzipping" behavior closely resembles the behavior of the SCCB during crack propagation. Therefore, the cohesive element was used to model the bond interface in the current study.

ABAQUS assumes that traction separation is linear elastic prior to undergoing complete damage evolution. The elastic behavior is represented by a constitutive matrix in terms of nominal stress and strain. While ABAQUS provides a three-dimensional model, torsional effects will not be presented here because only a two-dimensional model was employed. It should be noted that, while a mixed mode process may be present (normal and shear), the SCCB test inherently provides a Mode I failure which is predominantly normal to the interface.

Given that the nominal stress can be written as [18]

$$t_{ULT} = \left\{t_n^0\right\}, \tag{3}$$

where t is the total separation stress and t_n is the normal separation stress and strain can be written as

$$\varepsilon = \left\{\varepsilon_n\right\}, \tag{4}$$

where ε is the total separation strain and $\varepsilon_n = (\delta_n/T_o)$ is the normal separation strain, and T_o is the original thickness of the element, the elastic behavior can then be written as follows:

$$t_{ULT} = \left\{t_n^0\right\} = [K_n]\{\Delta_n\} = K_\varepsilon, \tag{5}$$

where K_n is the stiffness that relates to the nominal stress (N/m^3). The subscripts for the stiffness matrix represent again the normal separation (n).

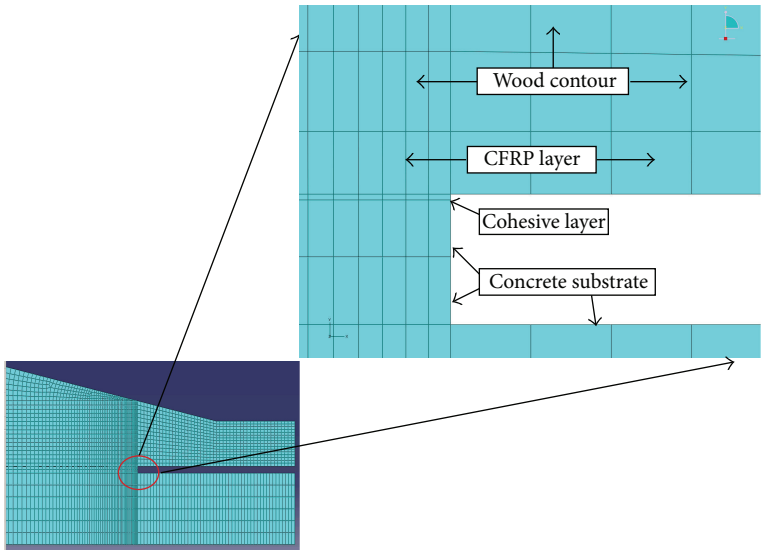

Figure 6: The finite element SCCB model.

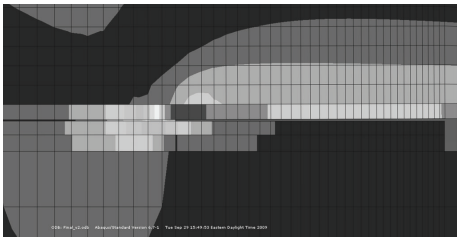

Figure 7: Close-up rendering of the damage evolution of the cohesive element.

Following the initial elastic response, damage is initiated provided that one of the user defined criteria is met. The damage initiation criteria can be defined in ABAQUS utilizing stress, strain, or quadratic function. The current work utilized a maximum stress criterion as follows [18]:

$$\max\left\{\frac{\langle t_n\rangle}{t_n^0}\right\} = 1, \tag{6}$$

where $\langle t_n\rangle$ is the normal stress state and t_n^0 is the peak normal stress.

Once the damage criterion is achieved, the material undergoes a softening process or loss of stiffness that perpetuates the damage evolution. ABAQUS [18] represents damage evolution by introducing the damage variable, D, which ranges in magnitude from 0 to 1. The effect of the damage variable is given by

$$t_n^0 = \begin{cases} (1-D)\, t_{\text{nd}} \\ t_{\text{nd}}, \end{cases} \tag{7}$$

where t_{nd} is the predicted normal stress (undamaged) and D is the damage variable.

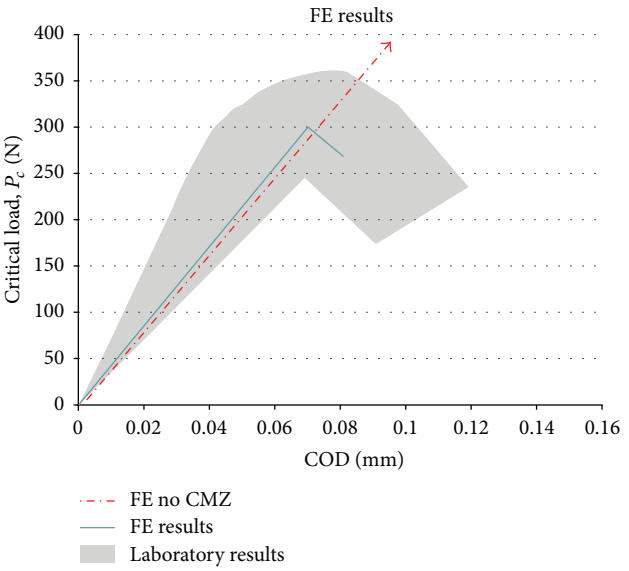

Figure 8: Finite element results compared to the companion laboratory results (straight line indicating nonseparation model with no CMZ).

4. Laboratory SCCB Tests

A series of SCCB tests was carried out [7]. The single cantilever contoured beam (SCCB) used for this study is comprised of a substrate material (reinforced concrete), a fiber-reinforced polymer layer, and a wood contour as illustrated in Figure 2. This study utilized the previously calibrated contour developed by Lawrence and Boyajian [7] with a rise of 95 mm.

As previously stated, the bonding substrate for the system is a reinforced concrete beam as illustrated in Figure 2. The target ranges for the concrete compressive strength were 27.58 ± 1.73 MPa, 34.50 ± 1.73 MPa, and 41.40 ± 1.73 MPa

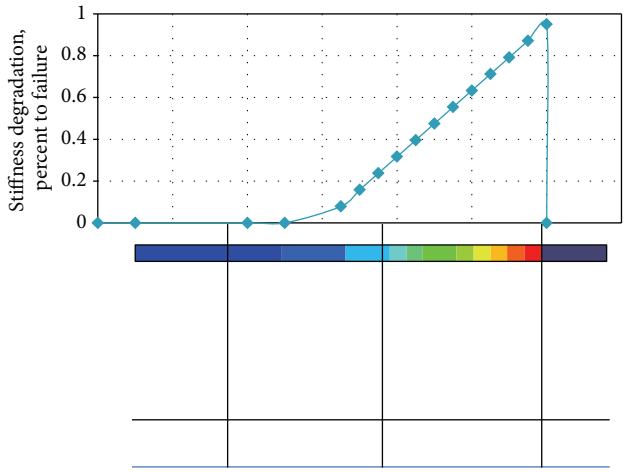

Figure 9: Stiffness degradation along the cohesive zone (crack propagation) including the stiffness degradation behind the crack.

among batches for consistency and comparison to previous work. The only derivation in testing protocol from previous studies was the mix design. The previous studies ([6, 7]) utilized approximately 1 : 1 : 1 and 1 : 2 : 4 ratios as the mix designs so as to increase the workability of the concrete into the mold and produce a consistent concrete surface. For the current work, the mix design was found using ACI 301 (2005) mix specifications which produced the more commonly used 1 : 3 : 5 mix design. While the issues of workability and a constant concrete surface are still true for the current study, they were addressed by employing a vibration table to fill voids and work the concrete into the mold. Additionally, a slump of 89 mm was used to further aid in workability. The only additive used in the mix design was an air entrainment agent which was added to achieve 6.5 percent ±1 percent average air content. The addition of an air entrainment agent was necessary due to future durability testing.

The testing regimen used by the entire study (compressive strength $f'c$ of substrate effects on G_C) required a total of nine concrete beam specimens. For each batching, the concrete was tested for slump, air entrainment, and compressive strength. The batch was considered successful if it met the mix design requirements previously defined. The average compressive strengths among the batches were 28.96 MPa (SD = 2.34 MPa), 36.89 MPa (SD = 0.10 MPa), and 40.85 MPa (SD = 0.10 MPa) with all batches meeting the compressive strength standards.

4.1. Fiber-Reinforced Polymer System. The fiber-reinforced polymer used in the study consists of two parts: the carbon fibers and epoxy. The system selected for the study was Sikadur 301 two-part epoxy and SikaWrap Hex 103C carbon fiber due to the system's increasing popularity in industry. The higher demand for the Sika 301 epoxy is a result of a lower cost for material and the lack of a primer coat, which in turn allows for faster construction times. The material properties for the system are listed in Table 1.

Table 1: Fiber-reinforced polymer properties (Sika).

	SikaWrap Hex 103C	Sikadur 301
Tensile strength	3.793 GPa	52.0 MPa
Tensile modulus	234.5 GPa	2.000 GPa
Elongation	1.5%	3.5% at break

4.2. Microllam Laminated Veneer Lumber. The contour material used in the study is a wood product, 1.9E Microllam LVL (laminated veneer lumber). The material was selected to serve as the contoured member of the SCCB specimen due to the ease by which it could be shaped as required by the compliance results (refer back to Figure 2). The material properties are listed in Table 2.

In employing the SCCB testing methodology [5], the success of determining the critical strain energy release rate is directly related to the accuracy of compliance. As first presented in the Irwin-Kies equation, compliance, C, is represented by a ratio of displacement to load increment. In the absence of a contoured cantilever, the compliance of the uncontoured beam changes as the crack location, a, propagates along the structural member. As a result, calculating the critical strain release energy can only be achieved by continuously measuring the crack location during the experiment which is a difficult task. As a means to avoid the arduous measuring of crack tip location, a contoured shape is utilized that causes the compliance to change linearly in conjunction with crack propagation along the interface [5]. This linear relationship removes the dependence of load, P, and strain energy release rate, G_I, from the crack tip location, a.

In determining the optimized contour dimensions and in an effort to simplify the procedure, the dimensions of the contour are prescribed prior to analysis, except for h_f (the height of the contour given in Figure 1 as 95 mm) which will be iterated in a finite element model (FE) to achieve several approximated contour shapes. The crack tip location begins at 51 mm (starter crack) loaded with 448 N and the corresponding contour deformation at the load location is recorded. The process is repeated for crack tip locations at 51 mm intervals up to 357 mm of specimen length. The resulting compliance, C (calculated as u/P), is plotted as a function of crack tip location, a. The slope of the linear relationship provides the compliance gradient, dC/da. Subsequently, for each h_f that yields acceptable compliance gradients, an experimental calibration must be performed to assist in the final optimization of the contour.

This study utilized the previously calibrated contour developed by Lawrence and Boyajian [7] which had an h_f = 95 mm. The contour was modeled in ANSYS in an effort to check the compliance gradient. The resulting gradient used for the fracture studies was $dC/da = 1.49 \times 10^{-5}\ \mathrm{N}^{-1}$ which compares well with Boyajian [5].

From the experimental study, three representative specimens (closest to G_{IC} averages) of the nine pull test results are presented in Table 3, where G_C and P_C for the three different tests are presented along with the averaged values. Figure 2(c)

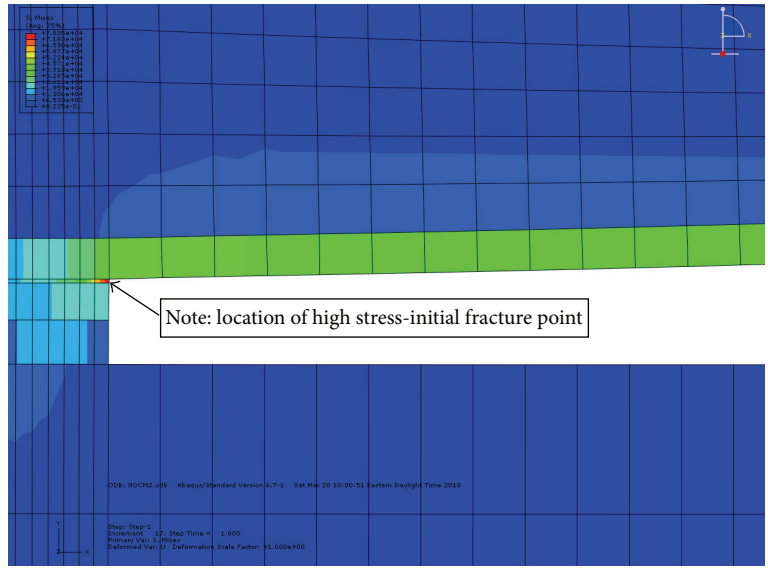

Figure 10: Stress distribution in the nonseparation model.

Table 2: 1.9E Microllam LVL properties.

Grade	G Shear modulus of elasticity	E Modulus of elasticity	E_{min} Adjusted modulus of elasticity	F_b Flexural stress
1.9E	819 MPa	13 GPa	6.6 GPa	18 MPa

Table 3: Representative experimental and analytical results.

Specimen	Critical load, P_c	G_{Ic} (initiation)	$F'c$
FRAC1031_T1	1494 N	384 J/m^2	37 MPa
FRAC1031_T2	1245 N	267 J/m^2	37 MPa
FRAC27_T3	1045 N	183 J/m^2	29 MPa
Average	1261 N	278 J/m^2	34 MPa
Finite element	1392 N	307 J/m^2	37 MPa

Table 4: Summary of FE material input values.

Material	Young's modulus	Poisson's ratio	Fracture energy
Concrete	30 GPa	0.18	N/A
LVL contour	13 GPa	0.30	N/A
Cohesive	102 GPa	N/A	134 J/m^2
CFRP	235 GPa	0.15	N/A

shows the typical failed specimens, where failure plane showed exposed aggregates embedded in the substrates. The failure plane for all tests fell within the concrete matrix and lied within the substrate. Figure 4 shows the critical load versus crack opening displacement from the test results.

5. SCCB Analytical Model

The SCCB was modeled using 2D plain strain plate quad elements in ABAQUS and represents the LVL contour, the concrete substrate, and the CFRP layer (see Table 4). For FRP laminates, typically orthotropic layer elements are used [1]; however, for the 2D model, nondirectional element is used.

The interface region was geometrically inputted to represent a mixed layer of concrete and epoxy due to the deep intrusion of crack propagation into the substrate. This interfacial zone was considered to be the cohesive layer and was modeled using ABAQUS cohesive element, COH2D4. The material properties required to model the cohesive element are G_c, K, nominal stress (traction), t, and separation, δ. The system was subjected to a 1.78 mm deflection of the contour tip, which corresponds to the laboratory results for the crack opening displacement (COD) at the critical load, P_c.

Figure 5 shows the FE model. Due to the deviation in concrete properties, averaged material properties from laboratory tests are used for the cohesive element: G_c = 133.97 J/m^2; K = 102.45 N/m^3 and nominal stress, 15.51 MPa. Table 3 provides a material summary for the SCCB model. The one area of concern in utilizing the cohesive element, as Duan et al. [19] pointed out, is the element size. Duan et al. [19] and others [12, 20] have proposed various analytical processes for determining cohesive element size and Diehl [17] proposed an element size of one-fifth of the model. The size of the cohesive element was 1/10 the size of the CFRP layer with an aspect ratio of 1 to 5. A close-up view of the final model is shown in Figure 6. It should be noted that the stress distribution at the location of the crack tip in Figures 5 and 7 ranged from 0 MPa to 48.46 MPa.

6. Results and Discussion

Figure 7 shows the stress distribution at critical load; significant crack propagation has penetrated into the interface. Over 50 cohesive elements have been removed (delamination) immediately after the critical load was achieved. Also illustrated in Figure 5, the stress distribution in the wood layer displayed typical Bernoulli bending behavior with compressive stresses of the cantilever at the top and the tensile stresses at the bottom. However, during the first fracture sequence of the SCCB, the interface was represented by a region of discontinuity as it pertains to the stress. The discontinuity is a result of the different material properties between the cohesive element, the concrete, and the FRP. The maximum stress in the FRP material is 48.46 MPa, which occurs at the crack tip, indicating that the composite wrap is being stressed.

Figure 8 shows the stiffness degradation within the interface (cohesive elements) and behind the crack. The analytical model produced reasonably close results compared to the laboratory results (Figure 8). Figure 8 is a rendering of the numerical model results as a function of all fractured specimens represented by the smeared gray area, indicating the experimental deviations. It should be noted that the laboratory results actually represent various compressive strengths of concrete, ranging from 29.0 MPa to 41.4 MPa. This will somewhat affect the specific fracture energy of the concrete as well as the effective stiffness of the cohesive layer.

The critical load, P_c, was determined to be 1392 N at a crack opening displacement of 1.78 mm. The averaged critical load from the laboratory results was 1261 N at a crack opening displacement of 1.70 mm, yielding a percent difference of approximately 9 percent and 4.5 percent, respectively. The critical strain energy release rate from the finite element analysis was then calculated as 307 J/m^2, which also corresponded well with the averaged critical strain energy release rate of 278 J/m^2, yielding a percent difference of 9.4 percent. While the numerical results are acceptable as the percent differences are within the laboratory specimen percent differences, the behavior of the modeled fracture varied somewhat from the laboratory results. The fracture produced in the model is more representative of stable crack propagation rather than the moderately unstable fracture pattern produced in the laboratory experiments.

Result from FE model with no cohesive material zone (CMZ) is also investigated, which shows significantly larger critical ultimate stress (straight line in Figure 9). Furthermore, there is a slight, but negligible, difference in stiffness between the two models. Figure 10 shows the stress concentration in the nonseparation model, where the peak stress at initial fracture point is 71.6 MPa. Since the model is not allowed to crack, the FRP composite does not demonstrate realistic stress distribution as indicated in Figure 6. It is also of interest to note that high stress concentration exists within the concrete elements during loading (Figure 5), accurately portrayed possible penetrating into the substrate.

7. Conclusions

The preceding work documents the effectiveness of modeling the delamination of CFRP that has been bonded to concrete utilizing the Abaqus defined cohesive element. The model does accurately predict the critical load, P_c, as well as the crack opening displacement, COD. Furthermore, without the use of the cohesive element, the stress distribution at the crack initiation cannot be modeled properly. The significance of the numerical modeling is the accurate portrayal of the debonding process of SCCB test method with SP3 surface: as was the case with the experiment results, the model bears out the deep penetration into the concrete substrate.

Comparing to the nonseparation model (without cohesive element), the peak stress is significantly higher than the actual experimental results and the FRP material does not appear to resist the pull loading.

There are a few areas need to be addressed to fully define the SCCB analytically.

(1) As multiple materials are contributing to the strength of the bond, it would be intuitive that each of these materials could be represented by multiple cohesive layers.

(2) One area of concern is the added concrete material to the contour during fracture. The addition of this material could impact the compliance.

(3) The nonhomogeneity of the wood and concrete caused some concern when comparing the numerical results to the laboratory results.

(4) Modeling the cohesive zone as a zero thickness element should be investigated for stiffness effects.

References

[1] V. Giurgiutiu, J. Lyons, M. Petrou, D. Laub, and S. Whitley, "Fracture mechanics testing of the bond between composite overlays and a concrete substrate," *Journal of Adhesion Science and Technology*, vol. 15, no. 11, pp. 1351–1371, 2001.

[2] V. M. Karbhari and M. Engineer, "Investigation of bond between concrete and composites: use of a peel test," *Journal of Reinforced Plastics and Composites*, vol. 15, no. 2, pp. 208–227, 1996.

[3] I. Kimpara, K. Kageyama, T. Suzuki, I. Osawa, and K. Yamaguchi, "Characterization of debonding energy release rate of FRP sheets bonded on mortar and concrete," *Advanced Composite Materials*, vol. 8, no. 2, pp. 177–187, 1999.

[4] D. M. Boyajian, J. F. Davalos, and I. Ray, "Evaluation of interface fracture of concrete externally reinforced with FRP," in *Proceedings of the 2nd International Conference on Durability of Fiber Reinforced Polymer (FRP) Composites for Construction (CDCC)*, Montreal, Canada, 2002.

[5] D. M. Boyajian, *Mode I fracture and durability of the CFRP-concrete interface bond [Ph.D. thesis]*, West Virginia University, 2002.

[6] S. S. Kodkani, *Interface durability of externally bonded GFRP to normal and high-performance concrete [M.S. thesis]*, West Virginia University, 2004.

[7] T. O. Lawrence and D. M. Boyajian, "Surface roughness, quasi-static fracture, and cyclic fatigue effects on GFRP- And CFRP-concrete bonded interfaces," *Journal of ASTM International*, vol. 3, no. 1, pp. 1–14, 2006.

[8] International Concrete Repair Institute, *Concrete Surface Preparation for Fiber Reinforced Polymers*, International Concrete Repair Institute, Des Plains, Ill, USA, 2003.

[9] O. Buyukozturk, O. Gunes, and E. Karaca, "Progress on understanding debonding problems in reinforced concrete and steel members strengthened using FRP composites," *Construction and Building Materials*, vol. 18, no. 1, pp. 9–19, 2004.

[10] J. P. Berry, "Determination of fracture surface energies by the cleavage technique," *Journal of Applied Physics*, vol. 34, no. 1, pp. 62–68, 1963.

[11] A. Boresi, R. J. Schmidt, and O. M. Sidebottom, *Advanced Mechanics of Material*, John Wiley & Sons, New York, NY, USA, 5th edition, 1993.

[12] A. Turon, C. G. Dávila, P. P. Camanho, and J. Costa, "An engineering solution for mesh size effects in the simulation of delamination using cohesive zone models," *Engineering Fracture Mechanics*, vol. 74, no. 10, pp. 1665–1682, 2007.

[13] G. R. Irwin, "Fracture," in *Encyclopedia of Physics*, S. Flugge, Ed., vol. 6, pp. 551–590, Springer, Berlin, Germany, 1958.

[14] G. R. Irwin and J. A. Kies, "Critical energy rate analysis of fracture strength," *Welding Journal Research Supplement*, vol. 33, pp. 193s–198s, 1954.

[15] T. Nicholas, *Mode 1 fatigue and fracture of the carbon fiber reinforced plastic to concrete bond interface region [Ph.D. thesis]*, University of North Carolina at Charlotte, 2010.

[16] D. Huang and J. Lyons, "Finite element analysis of test specimens to assess composite—concrete bond durability," *Journal of Reinforced Plastics and Composites*, vol. 24, no. 13, pp. 1387–1405, 2005.

[17] T. Diehl, "On using a penalty-based cohesive-zone finite element approach—part I: elastic solution benchmarks," *International Journal of Adhesion and Adhesives*, vol. 28, no. 4-5, pp. 237–255, 2008.

[18] ABAQUS Finite Element Code, Hibbitt, Karlsson and Sorensen, Inc., Providence, RI, USA, 2007.

[19] K. Duan, X. Z. Hu, and F. H. Wittmann, "Size effect on specific fracture energy of concrete," *Engineering Fracture Mechanics*, vol. 74, no. 1-2, pp. 87–96, 2007.

[20] A. M. Ibrahim and M. S. Mahmood, "Finite element modeling of reinforced concrete beams strengthened with FRP laminates," *European Journal of Scientific Research*, vol. 30, no. 4, pp. 526–541, 2009.